Available online at www.sciencedirect.com
SCIENCE DIRECT®
Journal of Sound and Vibration 286 (2005) 341–361
JOURNAL OF SOUND AND VIBRATION
www.elsevier.com/locate/jsvi

Indirect measurement of main bearing loads in an operating diesel engine

Q. Leclère[a,*], C. Pezerat[a], B. Laulagnet[a], L. Polac[b]

[a]*Laboratoire Vibrations Acoustique, INSA Lyon, 25 bis avenue Jean Capelle 69621 Villeurbanne Cedex, France*
[b]*RENAULT DM, 67 rue des bons Raisins 92500 Rueil Malmaison, France*

Received 26 November 2003; received in revised form 31 March 2004; accepted 5 October 2004
Available online 29 December 2004

Abstract

This paper deals with the application of indirect measurement techniques to an operating diesel engine. Internal loads exciting the engine block during operation are not directly measurable with force sensors; they have to be assessed from the dynamic deformation of the structure. The idea is to use the structure itself as a multi-force sensor, which requires the knowledge of the transfer functions between considered excitations and measured responses. The first part is devoted to the description of the methodology. In Section 1, the extraction of uncorrelated deflection shapes from stationary measurements is presented. Then the pseudo-inversion technique, needed to invert the transfer system, is reviewed. Optimization of the inversion, based on a weighing technique, is presented in Section 3. Then a regularization process based on the truncated singular value decomposition and the L-curve principle is suggested. In the second part, a basic model of a drive train is used to directly assess internal excitations from the measured cylinder pressures. Outputs of this model are compared with excitations indirectly measured on the operating engine in a third part. The efficiency of the optimization and regularization processes is illustrated, and encouraging results are presented, allowing information on defects of the drive train model to be obtained. Finally, a ranking operation is realized on internal excitations to illustrate the strong interest of the results of indirect force measurement.

*Corresponding author. Tel.: +33 4 72 43 63 92; fax: +33 4 72 43 87 12.
E-mail address: leclere@lva.insa-lyon.fr (Q. Leclère).

0022-460X/$ - see front matter © 2004 Elsevier Ltd. All rights reserved.
doi:10.1016/j.jsv.2004.10.027

0. Introduction

The indirect measurement of dynamic forces exciting mechanical structures is a research topic that has widely been explored since the end of the 1970s. Nevertheless, the direct measurement of exciting forces cannot be realized in many practical cases. Moreover, this piece of information is often necessary, as it is the case in machinery diagnostic for noise and vibration prediction. Unfortunately, this kind of inverse approach is known to be very sensitive to measurement and modeling errors. In this paper, we are interested in stationary vibrating systems for which excitation areas are a priori known. As a matter of fact, the industrial need of this study concerns the assessment of bearing loads inside an operating engine, more precisely on crankshaft bearings. The first section of this work describes the inverse method used, including a measurement post-processing technique to extract uncorrelated deflection shapes, and pragmatical optimization and regularization methods. The second section concerns the studied object: the diesel engine. A simple model of drive-train is suggested to directly simulate bearing loads from cylinder pressure measurements. Then, the last part has been dedicated to an experimental application on an operating diesel engine and presents encouraging results, showing the applicability of inverse methods to complex industrial systems.

1. Indirect force measurement method

1.1. Use of principal component analysis to identify incoherent phenomena

The first step in the characterization of a stationary vibrating structure is to determine the number of incoherent phenomena present on the measured response. The response of the structure is represented by the cross-spectral matrix made of auto and cross spectra of response sensors. If all responses are fully coherent with one another, close to unity, there is only one phenomenon which can be represented by a deflection shape. A deflection shape is defined by the complex deformation of the structure at the response points for a given frequency. In this case, phases between response points can be adjusted with regard to a chosen reference point

$$\begin{aligned} X_i &= \sqrt{S_{ii}}\mathrm{e}^{(\mathrm{j}\angle S_{ir})} \quad (i \in [1,\ldots,m] \text{ and } i \neq r), \\ X_r &= \sqrt{S_{rr}}, \end{aligned} \tag{1}$$

where $\mathrm{j} = \sqrt{-1}$, X_i is the ith element of the deflection shape $\{X\}$, S_{ii} the autospectrum of the ith response, S_{ir} the interspectrum between the ith response and the reference response, and $\angle S_{ir}$ the phase of the interspectrum S_{ir}.

If responses are only partially coherent between one another, it means that two or more incoherent phenomena are contributing to the deformation of the structure. For example, this is the case for the diesel engine in high frequency, when the forces created by the combustion in the four cylinders are no longer totally coherent, or for certain frequencies when the contribution of an accessory leads to a non-negligible level. Deflection shapes representing each phenomenon can be extracted from the entire cross-spectral matrix response by computing its decomposition using

eigenvalue and eigenvectors [1]

$$[S_{XX}] = [\Phi]^{\ulcorner} \Sigma^{\lrcorner} [\Phi]^*, \tag{2}$$

where $[S_{XX}]$ is the response cross-spectral matrix, $^{\ulcorner}\Sigma^{\lrcorner}$ the diagonal matrix of eigenvalues, $[\Phi]^*$ the complex conjugate transpose of $[\Phi]$ and $[\Phi]$ the matrix of eigenvectors arranged in columns.

The number of non-negligible eigenvalues, which can be considered as a physical rank of the cross-spectral matrix, corresponds to the number of incoherent phenomena contributing to the deformation of the structure. If all eigenvalues are significant, the number of incoherent phenomena might be greater than the number of eigenvalues. Anyhow, for indirect force measurement (IFM) application, the number of responses has to be greater or equal to the number of excitation points. Given that the number of incoherent phenomena is bounded by the number of input forces, the number of significant eigenvalues has to be lower or equal to the number of input forces. Let m and p be, respectively, the number of response points and significant eigenvalues. Assuming $^{\ulcorner}\sigma^2{}^{\lrcorner} = {}^{\ulcorner}\Sigma^{\lrcorner}$, we can write

$$[S_{XX}]_{mm} = [\chi]_{mp} [\chi]^*_{mp}, \tag{3}$$

where

$$[\chi]_{mp} = [\Phi]_{mp}{}^{\ulcorner}\sigma^{\lrcorner}{}_{pp}.$$

Each column of $[\chi]_{mp}$ is a deflection shape characterizing one of the p incoherent phenomena. These incoherent deflection shapes are produced by a set of p incoherent *virtual* sources. The term *virtual* source is used because each virtual source is not related to a *physical* one taken into account in the IFM (physical sources are possibly partially coherent). This decomposition of the response cross-spectral matrix is known as the principal component analysis. It is a powerful multi-channel measurement treatment method, used in many cases as a pre-processing tool, for transfer path analysis, structural intensity, or acoustical holography.

1.2. Pseudo-inversion of the transfer matrix

The response of the structure, at a given point to a given excitation, is the convolution product of the excitation time history by the structure impulse response. In the Fourier domain, this convolution becomes a simple product. The relation in the Fourier domain between a set of m responses and a set of n excitations is expressed by a matrix product function of the frequency ω

$$\{X_{(\omega)}\}_m = [H_{(\omega)}]_{mn} \{F_{(\omega)}\}_n, \tag{4}$$

where $\{X_{(\omega)}\}_m$ is the set of responses, $\{F_{(\omega)}\}_n$ the set of forces and $[H_{(\omega)}]_{mn}$ the transfer matrix.

Each element of the transfer matrix is the frequency response function (FRF) between one of the excitations and one of the responses. The IFM problem is to estimate $\{F_{(\omega)}\}_n$ from the knowledge of $\{X_{(\omega)}\}_m$ and $[H_{(\omega)}]_{mn}$. The main condition to solve such a problem is that the number of responses m must be at least equal to the number of forces n. There are other conditions to ensure the well-posedness of the problem: the number of modes participating significantly to the response has to be at least equal to n, and excitations have to be sufficiently distant from one another to be sure that they can be identified. In the case of systems with several

incoherent phenomena, Eq. (4) can be formulated including several columns

$$[\chi_{(\omega)}]_{mp} = [H_{(\omega)}]_{mn}[\varphi_{(\omega)}]_{np}, \tag{5}$$

with columns of $[\chi_{(\omega)}]_{mp}$ corresponding to incoherent deflection shapes and columns of $[\varphi_{(\omega)}]_{np}$ to the repartition of each *virtual* source on *physical* sources.

The inversion of Eq. (5) is realized through a classical least-squares approach, by computing the pseudo-inverse of the transfer matrix

$$[\varphi_{(\omega)}]_{np} = ([H_{(\omega)}]_{mn})^{+}[\chi_{(\omega)}]_{mp} \quad \text{with } m \geqslant n, \tag{6}$$

where

$$([H_{(\omega)}])^{+} = ([H_{(\omega)}]^{*}[H_{(\omega)}])^{-1}, \quad [H_{(\omega)}]^{*} \text{ is the pseudo-inverse of } [H_{(\omega)}].$$

It is obvious that Eq. (6) could be formulated separately for each column of $[\varphi_{(\omega)}]$ and $[\chi_{(\omega)}]$, but this global formulation is needed for further calculations (namely, the regularization process). Other least-squares methods, like total least squares, can also be used to solve Eq. (5), but are known to be more sensitive to model errors and to a high conditioning of the transfer matrix (see Ref. [2]).

The complete cross-spectral matrix of forces can finally be computed by summing the p incoherent processes

$$[S_{FF}]_{nn} = [\varphi_{(\omega)}]_{np}[\varphi_{(\omega)}]^{*}_{np}. \tag{7}$$

1.3. Optimization by weighting

Least squares is a numerical method used to find the solution to a problem minimizing the Frobenius norm of a so-called residual quantity. The residue $[R]$ is the difference between a priori and a posteriori deflection shapes, a priori deflection shapes designing the measured $[\chi]$ matrix and a posteriori ones the matrix $[\chi]$ resulting from Eq. (5):

$$[R_{(\omega)}] = [\chi_{(\omega)}] - [H_{(\omega)}][\varphi_{(\omega)}]. \tag{8}$$

The Frobenius norm of a matrix is given by

$$\|[R_{(\omega)}]_{mp}\|_{\text{fro}} = \sqrt{\sum_{i=1}^{m}\sum_{j=1}^{p} |R_{ij(\omega)}|^2}, \tag{9}$$

where $R_{ij(\omega)}$ is the jth element of the ith row of the residue $[R_{(\omega)}]_{mp}$.

The importance given to the elements of the residual matrix $[R_{(\omega)}]$ for its minimization depends on their magnitudes. Weights can be assigned to rows of the residual matrix to adjust the importance given to them. The assignment of weights to rows of the system is like adjusting the importance given to response sensors. Both sides of Eq. (4) are multiplied by a diagonal left-weighing matrix $\ulcorner W \lrcorner$

$$\ulcorner W \lrcorner_{mm}[\chi_{(\omega)}]_{mp} = \ulcorner W \lrcorner_{mm}[H_{(\omega)}]_{mn}[\varphi_{(\omega)}]_{np}. \tag{10}$$

When different units are allocated to sensors, or for heterogeneous structures, large differences can appear in the responses and residues. This can lead to neglecting the information provided by

responses showing the lowest magnitudes, for example, sensors placed on very stiff measurement directions. For the engine application, this is the case for sensors located on crankshaft bearings, since the vertical axis is much stiffer than the longitudinal one. A systematic weighing technique, suggested in Refs. [3,4], is used to overcome such difficulties. The weights are adjusted so that a set of uncorrelated unit forces can give a set of unit responses through the weighted transfer matrix

$$W_{i,i} = \sqrt{\left(\sum_{j=1}^{n} |H_{i,j}|^2\right)^{-1}} \quad \text{with } i \in [1,\ldots,m], \tag{11}$$

where $W_{i,i}$ is the ith element of the diagonal of $\ulcorner W \lrcorner$, and $H_{i,j}$ the jth element of the ith row of the transfer matrix.

Eq. (6) can finally be written with the weighted pseudo-inverse of the transfer matrix

$$[\varphi_{(\omega)}]_{np} = ([H_{(\omega)}]_{mn})^{W+}[\chi_{(\omega)}]_{mp}, \quad \text{with } m \geqslant n, \tag{12}$$

where

$$([H_{(\omega)}])^{W+} = (\ulcorner W \lrcorner [H_{(\omega)}])^{+}, \quad \ulcorner W \lrcorner \text{ is the weighted pseudo-inverse of } [H_{(\omega)}].$$

1.4. Truncated SVD regularization using the L-curve principle

In the case of high conditioning of the transfer matrix, the direct use of formulations described in previous sections can lead to erroneous results. High conditioning can appear in several ways

- Two or more excitations are too close (they are not separable because they are generating equivalent responses).
- The modal participation of the response is poor, e.g. in low frequency or in the vicinity of lightly damped resonant frequencies of the structure. The number of modes significantly participating to the response has to be at least equal to the number of unknown forces.

In all these cases, some linear dependencies are introduced between columns of the transfer matrix. The result is that several linear combinations of the transfer matrix columns could generate the measured deflection shapes, with equivalent residual quantities. A choice has to be made between these quasi-solutions. The strict application of (6) leads one to choose the solution with the smallest residue, but the magnitude of this solution is often too large to be realistic. Many solutions without significantly higher residues are in fact more realistic. The idea to add a choice criterion, based on the norm of the solution, is the basis of the regularization procedures. The most popular regularization methods are truncated singular value decomposition (TSVD) and Tikhonov. These two methods are based on the adjustment of a regularizing parameter, discrete for TSVD and continuous for Tikhonov. This parameter adjusts the importance given to the minimization of the residue norm, on one hand, and to the solution norm, on the other. Many methods are known to adjust the regularizing parameter. In this paper, an original method is implemented, based on the L-curve principle [5]. This method is used with a TSVD regularization, based on the singular value decomposition of the weighted transfer matrix

$$\ulcorner W \lrcorner_{mm}[H]_{mn} = [U]_{mn}\ulcorner S \lrcorner_{nn}[V]^{*}_{nn}, \tag{13}$$

where $\ulcorner S \lrcorner_{nn}$ is the diagonal matrix of singular values sorted in descending order, $[V]_{nn}$ the unitary matrix and $[U]_{mn}$ such that $[U]^*_{mn}[U]_{mn} = \ulcorner I \lrcorner_{nn}$.

Eq. (10) can be easily inverted, if all singular values are non-zero, by substituting the weighted transfer matrix by its SVD:

$$[\varphi_{(\omega)}]_{np} = [V]_{nn} \ulcorner S \lrcorner^{-1}_{nn} [U]^*_{mn} \ulcorner W \lrcorner_{mm} [\chi_{(\omega)}]_{mp}.$$

TSVD is based on zeroing the $(n-s)$ last elements of the diagonal matrix $\ulcorner S \lrcorner^{-1}_{nn}$, corresponding to the $(n-s)$ smallest singular values. The number s of kept singular values is the regularizing parameter. The regularized weighted pseudo-inverse of the transfer matrix $[H]^{RW+}$ can finally be written as follows:

$$([H]_{mn})^{RW+} = [V]_{nn} \begin{bmatrix} \ulcorner S \lrcorner^{-1}_{ss} & 0 \\ 0 & 0 \end{bmatrix}_{nn} [U]^*_{mn} \ulcorner W \lrcorner_{mm}. \tag{14}$$

The parameter s is a rank artificially given to the transfer matrix. It means that the system is assumed to be rank-deficient, and that an infinity of solutions could satisfy the basic system expressed by Eq. (5). The regularized solution obtained through Eq. (14) corresponds to the solution of minimal norm. The difficulty of the method relies in the adjustment of s. This can be done by adjusting a threshold for singular values to be kept, in function of uncertainties on a measured transfer matrix [6], or on both transfer and response data [7]. In this work, a pragmatical tool has been used to assess this parameter: the L-curve principle. This method, usually used with Tikhonov regularization [5,8], can be adapted for TSVD. This principle is based on the parametric curve with the residue norm (noted ρ) on the x-axis against the solution norm (noted η) on the y-axis, in function of the regularizing parameter s. This curve has two main parts, a vertical part for which the decrease of s causes a diminution of the solution norm η without a significant augmentation of the residue norm ρ, and a horizontal part for which the decrease of s causes a slow diminution of η, tending to zero, and a significant augmentation of ρ, tending to the response norm. The optimal point of the L-curve is its angle, for which the decrease of s has caused an important diminution of the solution norm η without a significant growth of the residue norm ρ. An example of an L-curve is shown in Fig. 1. The transfer matrix used for this example has 28 columns, each cross of the curve corresponds to a number s of kept singular values. The numerical implementation of the L-curve principle to assess the optimal value for s is not straightforward. A procedure has been established based on normalized values of the solution norm and the residue norm. The residue norm has been normalized with respect to the response norm. The solution norm has been normalized with respect to the norm of the non-regularized solution. Normalized values are noted, η_N and ρ_N, for the normalized solution norm and normalized residue norm

$$\rho_N(s) = \frac{\|\{X\} - [H]\{F\}\|}{\|\{X\}\|},$$

$$\eta_N(s) = \frac{\eta(s)}{\eta(n)},$$

where $\eta(n)$ and $\rho_N(n)$ are the values of the solution norm and the normalized residue norm for $s = n$ (i.e. no regularization).

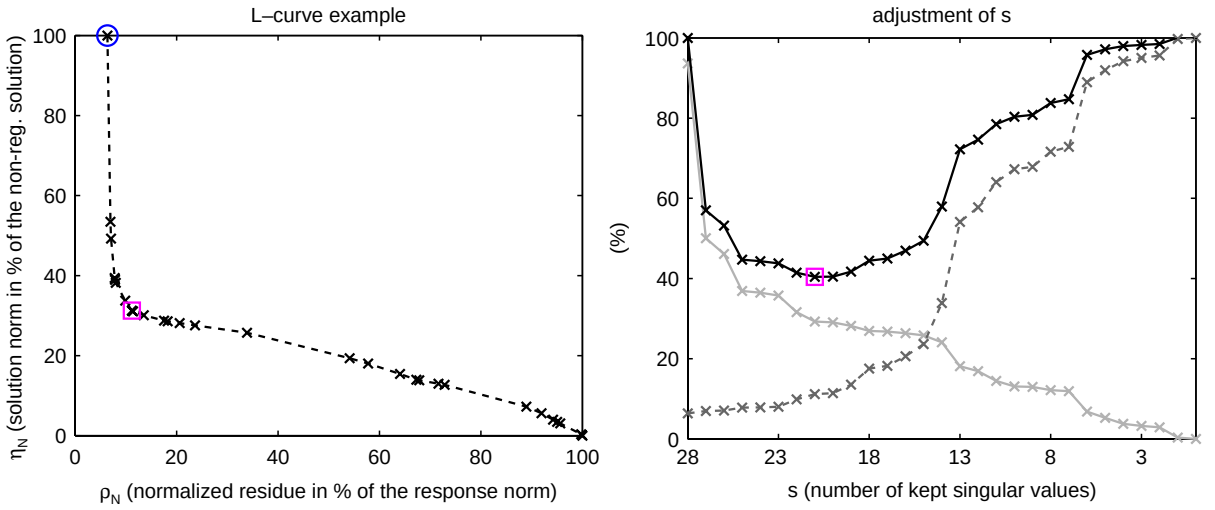

Fig. 1. Illustration of the L-curve principle. On the left: - -, L-curve, ○, no truncature ($s = n$). □, optimal truncature, s_{opt}. On the right: ——, $\xi(s)$, – –, $\rho_N(s)$, ——, $\eta_N(s)(1-\rho_N(n))$, □, minimum of $\xi(s)$ giving the optimal truncature s_{opt}.

An indicator $\xi(s)$ of the success of the regularization is introduced, based on the sum of ρ_N and η_N

$$\xi(s) = \rho_N(s) + \eta_N(s)(1-\rho_N(n)).$$

A corrective factor $(1-\rho_N(n))$ is introduced on $\eta_N(s)$ in order that $\xi(s)$ be equal to 1 for extremal values of s. The optimal number of kept singular values s_{opt} is considered to be the one minimizing $\xi(s)$. Quantities ρ_N, $\eta_N(1-\rho_N(n))$, and $\xi(s)$ are drawn in function of s in Fig. 1 (on the right), for the same case as the presented L-curve.

1.5. Summary of the IFM methodology

A global description of the indirect force measurement method is given in Fig. 2. On the one hand, the frequency response functions between excitation and response points have to be known, either from a model or from measure. A weighting matrix is computed in order to compensate large magnitude differences appearing in the transfer matrix (Section 1.3). On the other hand, time responses of the operating machine are acquired and stored into a cross-spectral matrix. A principal component analysis is performed to extract uncorrelated deflection shapes (Section 1.1). A singular value decomposition is realized on the weighted transfer matrix. The number of truncated singular values is then adjusted according to the L-curve principle (see Section 1.4). Uncorrelated excitation is then computed due to the regularized weighted pseudo-inverse expressed by system (14). The cross-spectral matrix of forces can finally be obtained by application of Eq. (7).

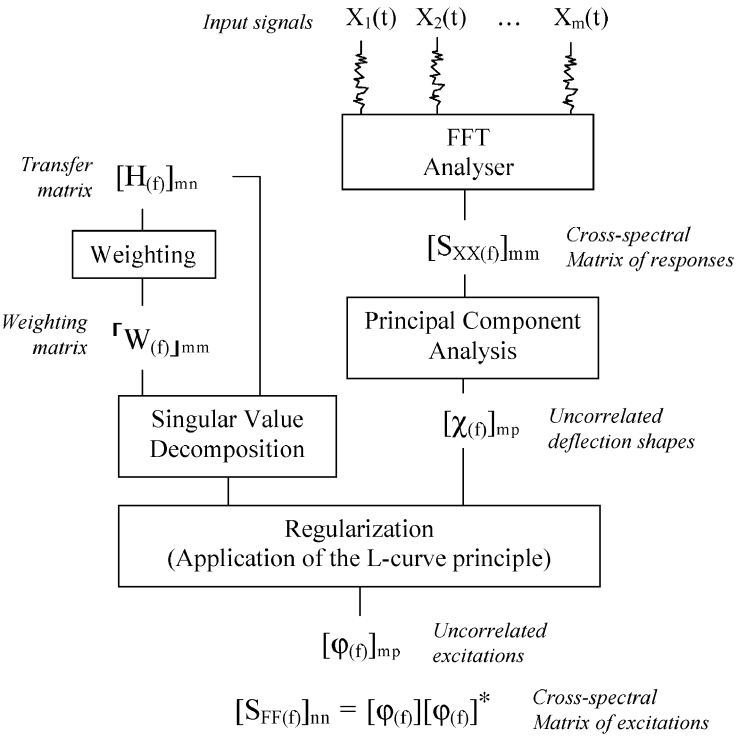

Fig. 2. General scheme of IFM.

2. Model of the diesel engine

2.1. Considered internal excitations

The studied system is a Renault 1.9L DCI engine (F9Q) with four in-line cylinders. The transfer case is bolted on the cylinder block, but it is empty of any gears and the drive shaft is directly connected to an electric power brake. The drive train (pistons, connecting rods and the crankshaft) is considered as an exciting part, therefore it is exterior to the transfer system.

First, all significant vibration sources of the operating engine have to be inventoried

- combustion gases exciting the cylinder head,
- piston forces on cylinder liners,
- vertical and horizontal forces applied by the crankshaft on the main bearings,
- vertical and horizontal moments applied by the crankshaft on the main bearings.

Some hypotheses are made about the first two types of exciting forces, all of them coming from the fact that excitations on both the cylinder head and cylinder liners are impact-like forces. As a matter of fact, combustion forces are explosions, arising for each cylinder when the piston is close to top dead center (TDC). In diesel engines, the compression rate has to be relatively high in

comparison with the gasoline ones, and the piston is very close to the cylinder head at the TDC. That is why it is assumed that combustion forces are exciting the cylinder head only, and the tops of cylinders are not taken into account.

Three different physical phenomena are superimposed for forces applied by pistons on cylinder liners

- combustion forces traveling through the pistons,
- inertial forces of the drive train,
- piston-slap.

Inertial forces result from alternative and rotative masses of the drive train. These forces are almost sinusoidal ones, and can be thought to be significant, but only for very low frequencies, on the first harmonics of the engine speed. The piston-slap is an impact force generated by piston-liner clearances. The piston moves from one side of the cylinder to the other one when the resultant force changes sign, generating an impact. This phenomenon appears several times per cycle, but the most significant shock is when the change of inclination of the connecting rod is coupled to high pressure in the combustion chamber, i.e. at the same time as the combustion process. Lastly, piston-liner forces are considered to be injected at only one point of the thrust-side of the cylinder liner, at 30 mm of the cylinder head. This area corresponds approximately to the piston-slap impact zone, and also to the position of the reaction force induced by the combustion.

All the forces being taken into account are summarized in Fig. 3.

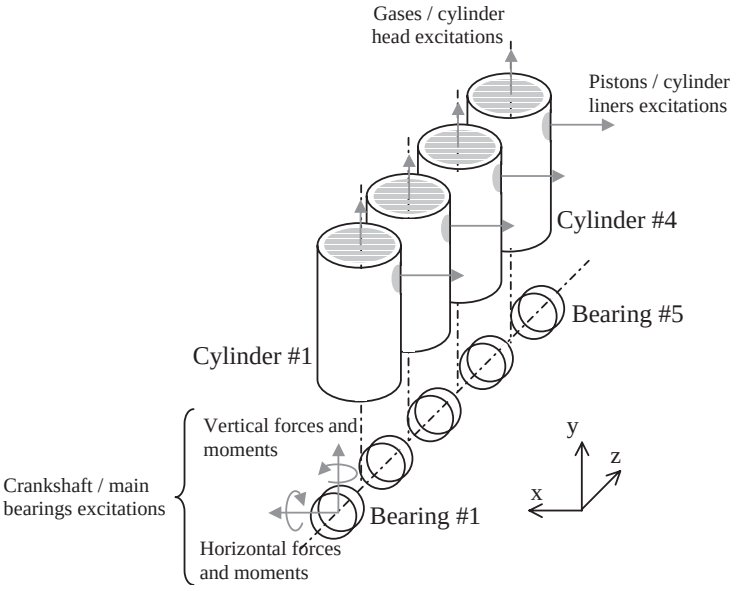

Fig. 3. Excitation model of the engine.

2.2. Transfer model

A finite element model of the engine is used to compute transfer functions. The model is made of 30 000 3D and 40 000 2D elements. A modal basis is computed from 0 to 10 kHz, including pseudo-static modes on excitation directions to take residual stiffnesses into account. Modal damping is approximately added by frequency bands in comparison with some transfer functions measured on the real engine (5% below 600 Hz, 3% between 600 and 2000 Hz and 1% above 2 kHz). Computed transfer functions are considered to be realistic ones up to 3 kHz. An example of a computed transfer function, with an excitation and a response on bearing 3 (y-axis) is compared with a measured one in Fig. 4. The transfer matrix assessment is the crucial point of IFM methods. It can be either measured or computed with a model. If the transfer matrix is based on measurements, some uncertainties appear; because of the complexity of involved excitation devices, or because the transfers are acquired by reciprocity. If the transfer matrix is based on finite element computations, model error is obviously present, and some updating (at least for damping) is needed. The reliability of reconstructed excitations will depend on the transfer model accuracy, and special care will have to be given to this modeling step. These considerations are more deeply investigated in Ref. [9].

2.3. Excitation model

An excitation model is used to compute internal forces from the measured cylinder pressures to assess the relevance of indirectly measured forces. Gas forces are directly injected into the cylinder

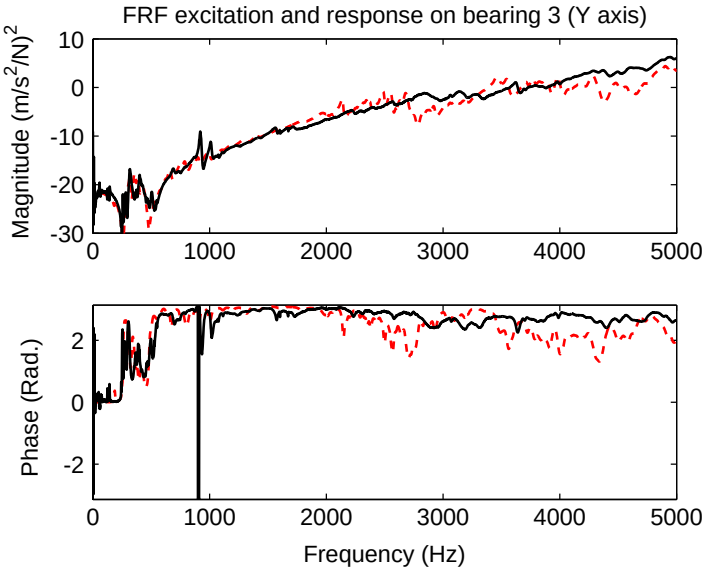

Fig. 4. Comparison between computed ___ and measured FRF - - -.

head through the exposed surface area. A dynamic model of a mono-cylinder with a rigid piston and a rigid connecting rod is used to determine forces transmitted to cylinder liners and crank pins [10]. A pseudo-static crankshaft model is used to distribute crank pin forces on the main bearings of the cylinder block. This model is made of simple beams and is updated on static bending and torsional deformation measurements. Each beam modeling a crankshaft journal is blocked on its two nodes in translation on two axes to simulate a rigid bearing. One extremity of the model is blocked in rotation to simulate the transmitted torque. An example of static force transmission from crank pin #3 to the five bearings is drawn in Fig. 5. This excitation model is very simple and is assumed to give a first approximation of internal excitations which can be compared to indirectly measured forces.

Gas pressure measured in the four cylinders is used to compute forces injected into the structure during one cycle. The Fourier transform of forces taking a time window of one engine cycle is equivalent to a Fourier series on multiples of the half engine speed. The magnitude of those Fourier transforms, equivalent to instant autospectra, is computed for each cycle and ensemble averaged for 1 min. An example of measured cylinder pressure in cylinder #3 and #4 during one cycle is drawn in Fig. 6 (on the left) with the resulting y-axis force on bearing #4 (on the right) and the corresponding ensemble-averaged autospectrum (at the bottom). The engine speed is 3500 rev/min with a 164 Nm torque transmitted to the power brake. The y-axis force on bearing #4 is drawn with and without gas loads for both the time history and the frequency spectrum, to show the difference between inertial and combustion forces. It is noted that the autospectrum of the force having only inertial loads is concentrated on entire harmonics of the engine speed, because without gas loads, one engine cycle corresponds to two periods of the excitations. The extinction of odd harmonics of the spectrum having gas loads is caused by the repetition of two similar patterns (gas explosions in adjacent cylinders #3 and 4) with a delay of a half engine rotation.

The mean engine torque, computed for each cycle with the excitation model, is 195 Nm, that is to say 20% greater than the measured one. The difference can be attributed to mechanical friction losses that are not taken into account in the model.

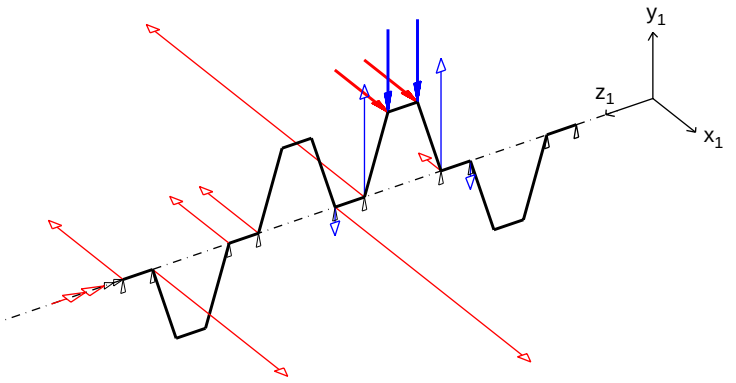

Fig. 5. Transmission of excitation on crank pin #3 to crankshaft bearings.

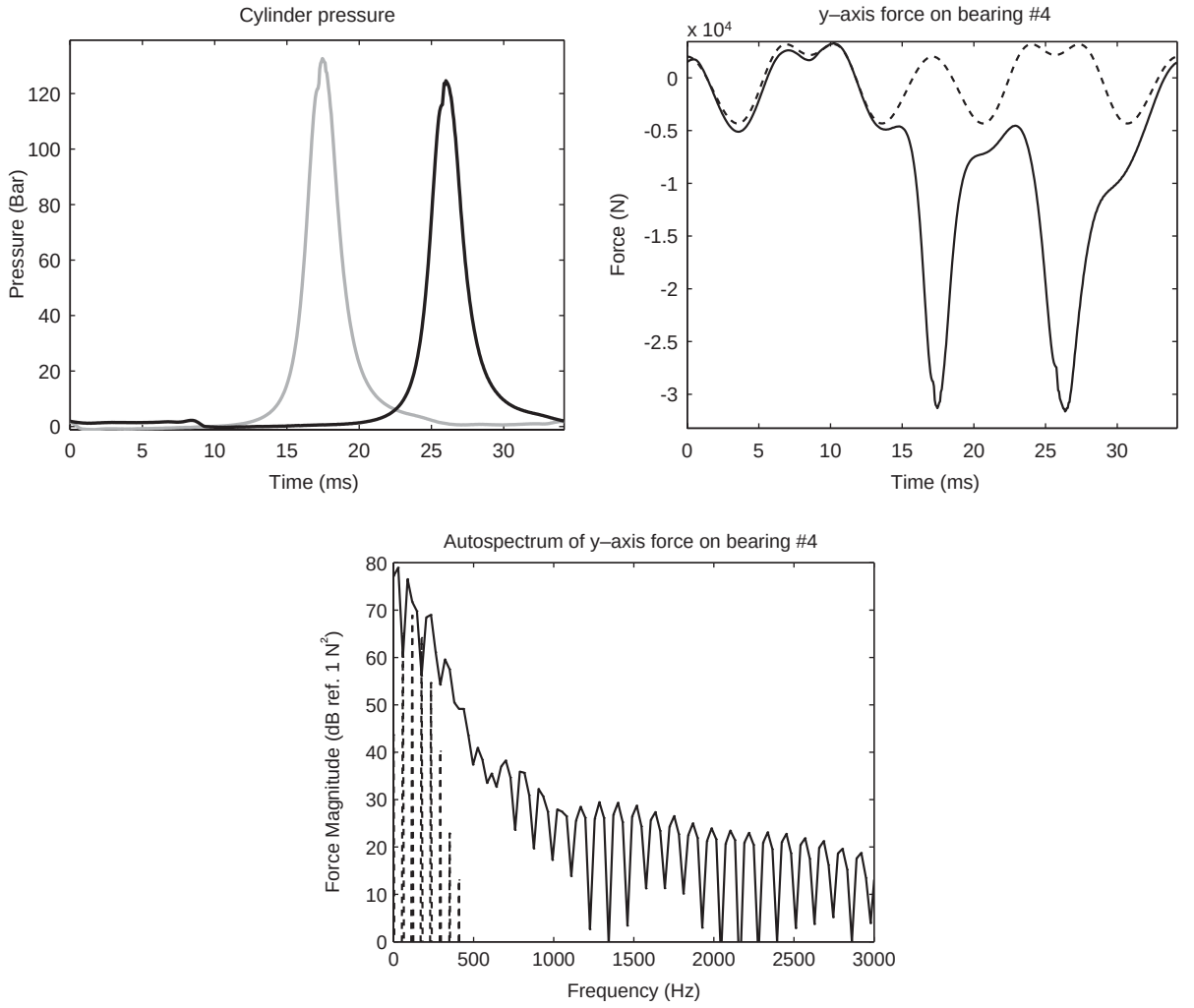

Fig. 6. Operating point (3500 rev/min/164 Nm). On the left: measured cylinder pressures —— #3 and —— #4. On the right: computed y-axis force on bearing #4, - -, without gas loads, ——, with gas loads. At the bottom: resulting y-axis force autospectrum on bearing #4, - -, without gas loads, ——, with gas loads.

3. Experimental application

3.1. Experimental setup and postprocessing of measurements

3.1.1. Setup

An engine bench is used to measure the operational responses of the structure. The crankshaft is directly connected to an electric power brake to control the engine torque. A 32-channel system is used to realize acquisitions. Four pressure sensors are placed in the four cylinders through the cylinder head. These sensors, measuring the pressure in the combustion chambers, are used to

Fig. 7. Bearing cap accelerometers.

directly estimate the forces injected to areas to the explosions. The 3D response of the five crankshaft bearing caps is measured with 14 heat-resistant accelerometers (response of bearing #1 is measured on only two axes). A picture of equipped bearings #2–5 is given in Fig. 7. The 14 remaining channels are connected to accelerometers placed on external faces of the engine. Six of them are distributed at the bottom of the skirt, four are placed in front of the cylinders on the thrust side, three are distributed on the anti-thrust side, and last one is fixed on the cylinder head.

3.1.2. Postprocessing of measurements

Acquisitions are done for several operating points; a point is characterized by both engine speed and engine torque. The 32 time history records of 1 mn length are stored with a frequency sampling of 16 kHz for each operating point. The entire cross-spectral matrix is then computed with a time window of 1 s (using a Hanning weighting). This 32*32 matrix of course depends on the frequency, with a resolution of 1 Hz. A principal component analysis is realized over each cross-spectral matrix following Eqs. (2) and (3), which allows us to write:

$$[S_{XX}]_{mm} = [\chi][\chi]^* = \sum_{i=1}^{32} \{\chi\}^i (\{\chi\}^i)^*. \tag{15}$$

We can then define the average rate of energy (over the 32 channels) coherent with the n first PCs (principal components):

$$\langle \gamma_c^2 \rangle_{c\in[1,\ldots,32]} = \left\langle \frac{\sum_{i=1}^{n} \chi_c^i \overline{\chi_c^i}}{S_{cc}} \right\rangle_{c\in[1,\ldots,32]}, \tag{16}$$

with $\langle A_c \rangle_{c\in[1,\ldots,32]}$ denoting the average value of A_c with c varying between 1 and 32, χ_c^i the cth component of vector $\{\chi\}^i$, $\overline{\chi_c^i}$ denoting the conjugate of χ_c^i and S_{cc} autospectrum of channel c.

γ_c^2 is the expression of the multiple virtual coherence of channel c with the n firsts PCs. The quantity expressed by (16) is given in Fig. 8 for three different operating points, with $n = 1$ on the left, and $n = 4$ on the right. It can be seen in Fig. 8 that the correlation level of the 32 channels depends on both the engine speed and the engine load. When the load and the speed are high (op. point 3500 rev/min/164 Nm), only one PC is needed to represent almost 90% of the total

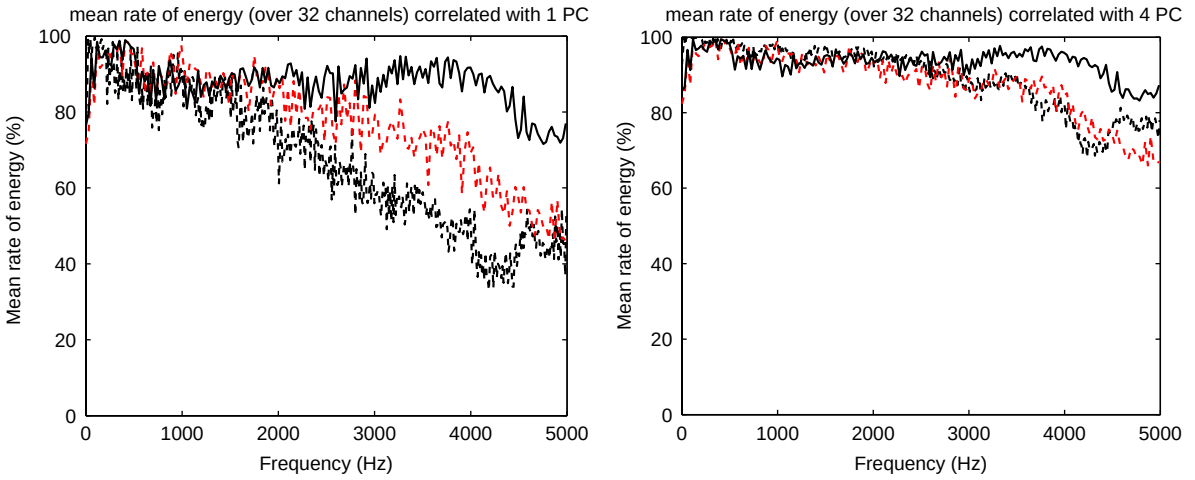

Fig. 8. Rate of energy correlated with 1 (on the left) and 4 (on the right) principal components. (1400 rev/min/38 Nm) - -, (3500 rev/min/40 Nm) – –, (3500 rev/min/164 Nm) ——.

energy from 0 to 5 kHz. Operational points having smaller engine speed or load ((3500 rev/min/40 Nm) or (1400 rev/min/40 Nm)) are more distributed over PCs, especially at high frequency. The mean rate of energy coherent with the first four PCs is represented in Fig. 8 (on the left). Four PCs are sufficient to keep a mean rate of energy above 90% up to 3 kHz for all operating points. Each cross-spectral matrix (size 32*32 function of frequency) representing an operating point is then decomposed into four incoherent deflection shapes (size 32*4 function of the frequency, following Eq. (3) with $p = 4$) before applying the inverse force determination process.

3.2. Indirect measurement of engine internal excitations

3.2.1. Injection of directly measured excitations as a priori information

Cylinder pressures constitute 4 of the 28 excitations described in Section (2.3). The introduction of measured cylinder pressures as a priori information reduces the conditioning of the problem (a similar approach is used in Ref. [11]). This operation is realized by adding four rows to the transfer matrix constructed in Section (2.2). The expression of Eq. (4) is then given by the following system (for one given deflection shape at one given frequency):

$$\left\{\begin{array}{c} P_1\ (\mathrm{Pa}) \\ P_2 \\ P_3 \\ P_4 \\ \hline \\ X_1\ (\mathrm{m.s^{-2}}) \\ \vdots \\ X_{28} \end{array}\right\} = \left[\begin{array}{ccccccc} S^{-1} & 0 & 0 & 0 & 0 & \dots & 0 \\ 0 & S^{-1} & 0 & 0 & 0 & \dots & 0 \\ 0 & 0 & S^{-1} & 0 & 0 & \dots & 0 \\ 0 & 0 & 0 & S^{-1} & 0 & \dots & 0 \\ \hline & & & & & & \\ & & & H & & & \end{array}\right] \left\{\begin{array}{c} P_1\ (\mathrm{N}) \\ P_2 \\ P_3 \\ P_4 \\ F_1\ (\mathrm{N}) \\ \vdots \\ F_{24} \end{array}\right\}, \tag{17}$$

where P_i is the cylinder pressure # i, X_i the response of accelerometer # i, S the surface area

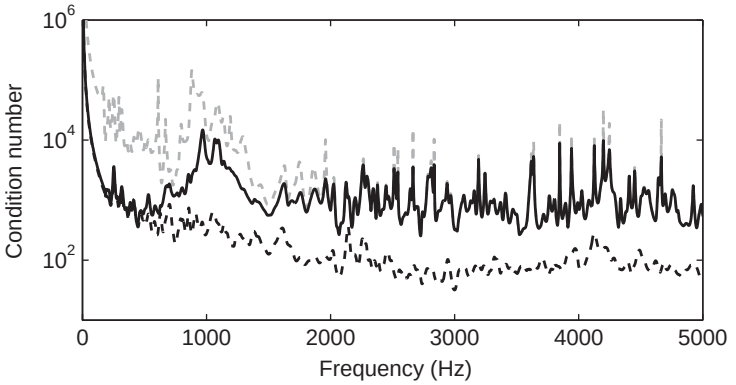

Fig. 9. Condition number for different transfer matrices (TMs): ___, 32*28 TM; _ _ 28*28 TM; - -, weighted 32*28 TM.

exposed to combustion, H the transfer matrix between the 28 excitations and the 28 responses and F_i the ith internal excitation other than cylinder pressure.

The condition number of the transfer matrices with (32*28) and without (28*28) the injection of cylinder pressure as a priori information is presented in Fig. 9. It is clear that the conditioning of the system is improved by this operation, particularly below 2 kHz. The condition number of the weighted transfer (32*28) matrix (according to Section 1.3) is also shown in Fig. 9. The decrease of the conditioning due to the weighting process is significant.

3.2.2. Comparison between the excitation model and the indirect force measurement on crankshaft bearings

Eq. (17) is solved for each frequency and each operating point. For all computations, the first four principal components of the cross-spectral matrix are retained. Both the weighting process described in Section 1.3 and the regularization process described in Section 1.4 are systematically applied. The number of truncated singular values is relatively constant over both the operating points and frequency. The mean number of truncated singular values is 2.7, with a standard deviation of 1.5. Forces obtained by indirect measurement are compared to forces computed with the model developed in Section 2.3. Autospectra obtained by indirect measurement have the same frequency resolution as the measured responses, that is to say 1 Hz. We are interested in autospectra corresponding to the diagonal of the excitation cross-spectral matrix (see Eq. (7)). They correspond to the global process, i.e. the sum of the four incoherent processes. They are integrated by frequency bands with central frequencies corresponding to the harmonics of half engine speed to compare them with results of the excitation model. Some results are presented in Figs. 10 and 11 for operating points 1400 rev/min/38 Nm and 3500 rev/min/164 Nm. For each figure, the results obtained with and without the optimization processes (normalization and regularization) are drawn to show the correction resulting from optimization.

The figures show that the correction applied by optimization is significant for frequencies above 1 kHz. The correction can reach more than 25 dB on certain harmonics, which shows the strong interest of normalization and regularization.

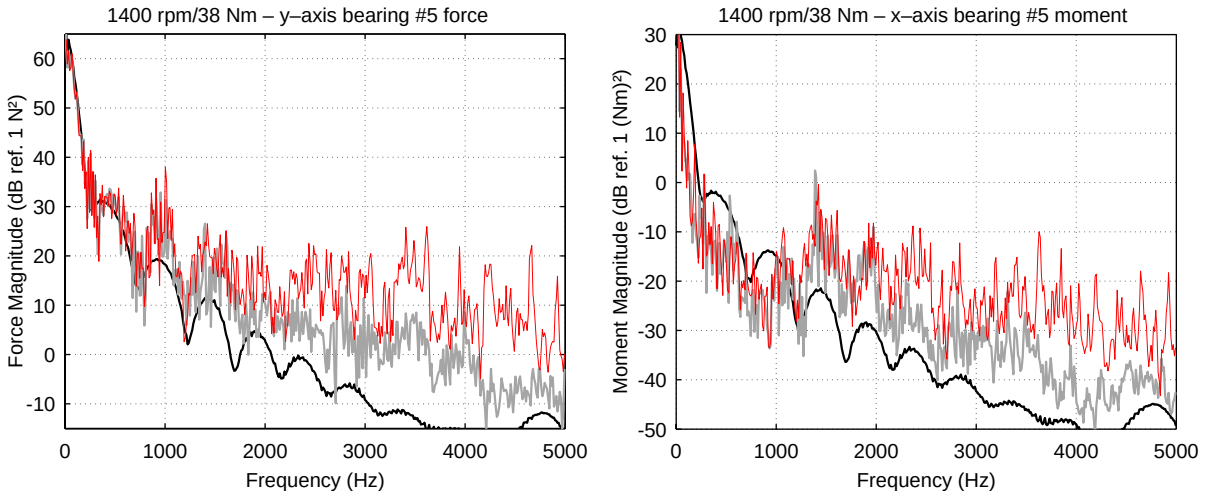

Fig. 10. Comparison between excitation model ——, and indirect measurement (—, without optimization; ——, with optimization) on bearing #5 for operating point (1400 rev/min/38 Nm).

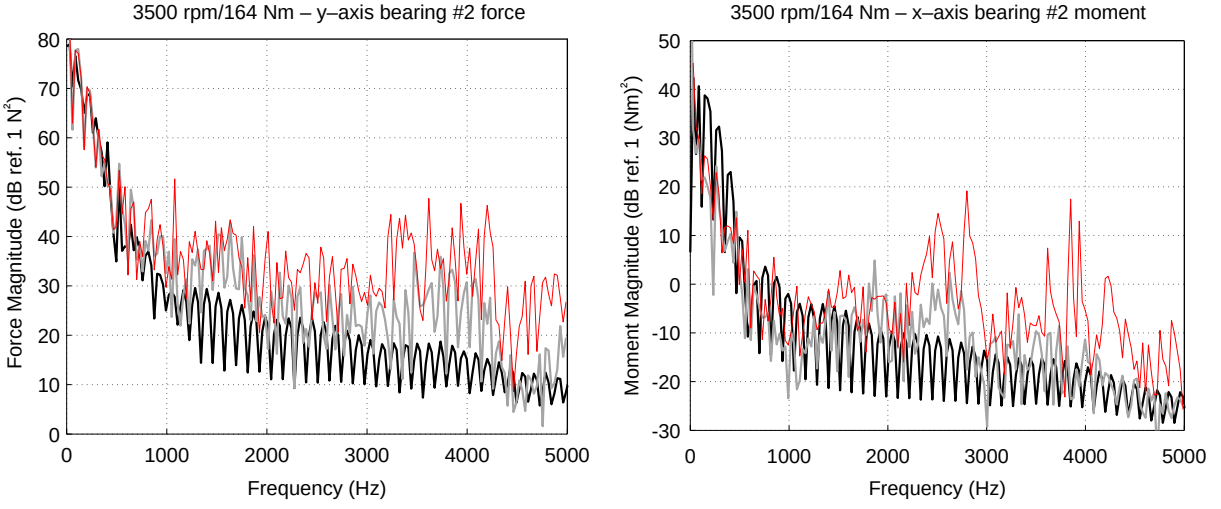

Fig. 11. Comparison between excitation model ——, and indirect measurement (— without optimization, —— with optimization) on bearing #2 for operating point (3500 rev/min/164 Nm).

The y-axis force and the x-axis moment on bearing #5 are shown in Fig. 10. It can be noted that the reconstructed force is well correlated with the simulated one, particularly at low frequency (below 800 Hz). This observation confirms that the order of magnitude of indirectly measured forces is realistic, and that the regularization process is suitable. Above this frequency range, the indirectly measured force is greater than the simulated one. This difference can be attributed to the low frequency nature of the excitation model, which does not take either modal deformation

of the drive train or clearances in joints between moving and static parts into account. The result of the indirect measurement can consequently be considered to be more realistic. Concerning the x-axis moment, the indirectly assessed one is lower than the modeled one at low frequency. This difference is attributed to the stiffness error of the crankshaft model in this direction. As a matter of fact, the flexibility of bearings is not taken into account; they are assumed to be completely rigid. This approximation is suspected to overestimate the x-axis moments applied by the crankshaft to the bearings. The frequency range of this effect corresponds to the part of the spectrum that is under the first bending mode of the bearings (in the vicinity of 1 kHz), that is to say, when bearings are excited in stiffness. Above 1 kHz, the indirectly measured moment is greater than the simulated one, which confirms the frequency limitation of the model.

Concerning the operating point (3500 rev/min/164 Nm) (see Fig. 11), equivalent comments can be made. The bearing being considered is #2, which explains the more complex shape of the autospectra (extinction of some harmonics): excitations on bearing #2 mainly result from the combination between explosions on the two adjacent cylinders (#1 and 2), which induces phase effects on some harmonics. These effects are not visible on bearing #5 which is adjacent to cylinder #4 only.

3.2.3. *Identification of excitations applied by pistons on cylinders*

The autospectrum of the identified excitation on cylinder #4 is given in Fig. 12 for operating point (1400 rev/min/72 Nm), and compared with the result of the excitation model. In very low frequency (below 200 Hz), the indirect measurement and the excitation model have the same order of magnitude. Above 200 Hz, both curves have equivalent slopes, but the indirect measurement is about 25 dB greater than the excitation model. This very large difference could be explained by the fact that piston-slap is not taken into account in the model, piston–cylinder assemblies being considered as perfect (see part 2.1). However, it would be hazardous to say that the large difference observed between the two curves results from flaws in the excitation model only. The

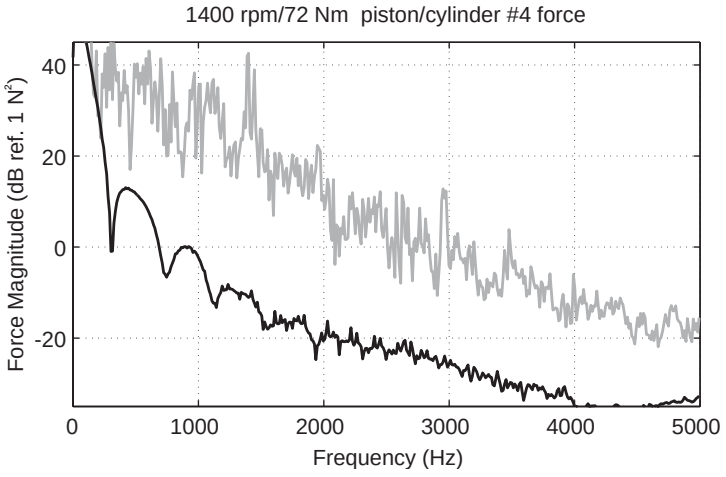

Fig. 12. Comparison between excitation model ___ and indirect measurement ___ on cylinder #4 for operating point (1400 rev/min/72 Nm).

result of IFM on cylinders has to be taken with precautions too. Response sensors are indeed not ideally placed to identify finely those excitations. Four accelerometers are placed on external faces of the engine block (on the thrust side), just in front of each cylinder. Between the external wall and the cylinder itself, there is cooling water. Thus, the sensors are not directly in contact with the cylinders, and the transfer system between the cylinder excitations and the four sensors can be thought to be insufficiently diagonal. The direct location of the sensors on cylinders through the external wall and the cooling water would have undoubtedly improved the results, but the experimental implementation would have been much more complicated.

3.2.4. *Computation of bearing excitations/cylinder pressures transfer functions*

The cross-spectral matrix of excitations resulting from IFM computations can be used to compute the transfer functions between internal forces. For example, transfer functions (TFs) between combustion forces and bearing excitations can be assessed. Such information can be useful to characterize the dynamic behavior of the mechanical filters existing between the combustion and bearings, i.e. pistons, connecting rods, and the crankshaft. The four combustion processes are totally coherent in low frequency, and partially coherent in high frequency. Thus, TFs between the combustion in one cylinder and bearing forces cannot really be obtained. However, bearings #1 and #5 are mainly excited by only one explosion, respectively, in cylinders #1 and #4 (other bearings are excited by their two adjacent cylinders). The TF between, e.g. combustion in cylinder #4 and vertical force on bearing #5 can then be roughly assessed, assuming that the combustion in cylinder #4 is the major excitation. TFs between the combustion in cylinder #4 and *y*-axis force/*x*-axis moment on bearing #5 are presented in Fig. 13 for different operating points. The cylinder pressure is expressed in Newton via the piston area. The estimator H1 is used to compute TFs, i.e. the ratio between the cross spectrum and the reference autospectrum. The mechanical filter constituted by the piston, the connecting rod and the

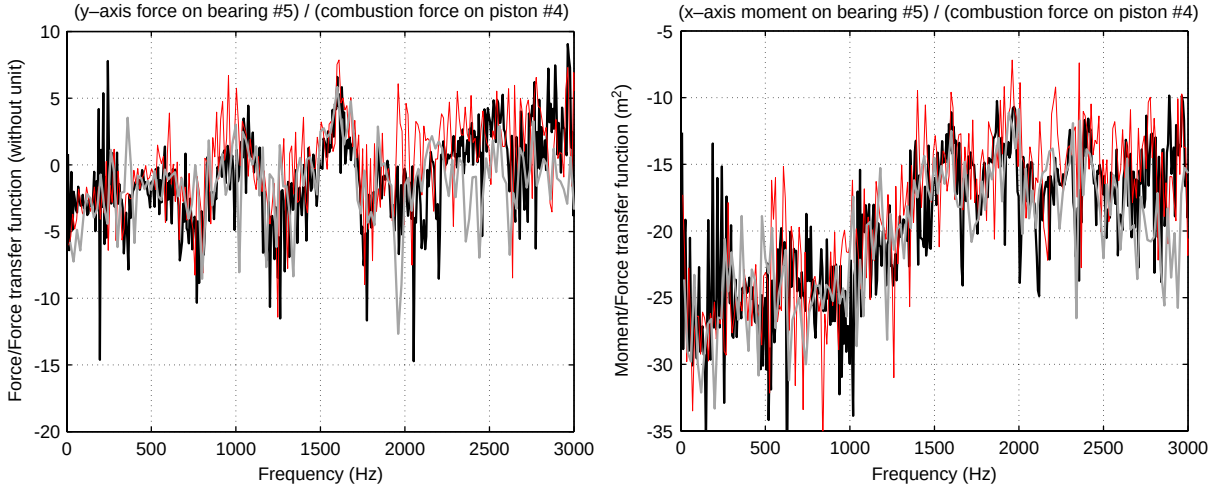

Fig. 13. Transfer functions between *y*-axis force (left) — *x*-axis moment (right) on bearing #5 and combustion force on piston #4. ___, idle; — (1400 rev/min/23 Nm); — (2400 rev/min/16 Nm).

crankshaft is suspected to have a nonlinear dynamic behaviour, because of unperfect joints and oil films existing between components. The aim of this paper is not to study this nonlinear characteristic, that is why only low load operating points are used for TF computations. TF between combustion in cylinder #4 and y-axis force on bearing #5 is shown in Fig. 13 (on the left). The first observation is that for the three operating points at 810, 1400 and 2400 rpm, TFs have approximately the same shape below 2 kHz. A modal behavior can be identified, with modes at about 300, 600, 1000 and 1600 Hz. This relative concordance between different operating points indicates that IFM results are reliable, at least for vertical forces on bearings. The force–force transfer functions tend to −3 dB in low frequency. It corresponds to a division by 2, the combustion force in cylinder #4 being physically distributed on bearings #4 and #5.

TF between combustion in cylinder #4 and x-axis moment on bearing #5 is given in Fig. 13 (on the right). The differences between TFs computed for the three operating points are more important than for the y-axis force. Nevertheless, some general trends can be observed. TFs are comprised between −27 and −22 dB below 1 kHz, and between −17 and −12 dB above 1.5 kHz. These TFs are ratios between moments in Nm and forces in N, and they are consequently equivalent to lever lengths expressed in m. Below 1 kHz, this length is about 3 mm (−25 dB), and about 3 cm (−15 dB) above 1.5 kHz. It means that the TF between combustion and x-axis moment on the bearing is roughly 10 times greater in high frequency than in low frequency, the separation corresponding to the bending mode of the bearing, around 1100 Hz. The distance between the bearing center and the cylinder axis is about 4.5 cm, which corresponds to the static lever length if the crankshaft was supported by bearing #5 only.

3.2.5. *Ranking the contributions of internal excitations to the structure response*

An important application of IFM results consists in ranking the contributions of the identified excitations to the structure response. For the ranking process, excitations can be gathered in groups:

- combustion/cylinder head forces,
- piston/cylinder forces,
- bearing excitations.

For each group, a partial response of the structure is computed with Eq. (5). A global response is also computed with the complete force matrix. The sum of acceleration autospectra on the three axes at the belt side engine mount is presented in Fig. 14 for operating points 1400 rev/min/23 Nm (low speed, low load) and 3500 rev/min/164 Nm (high speed, high load). Results are presented by frequency bands of 250 Hz width to facilitate their interpretation.

A first observation is that when a ranking operation is realized on correlated excitations, partial responses can be greater than the global one. Partial responses can indeed have opposite phases, especially if excitations are antagonist, e.g. gas/cylinder head and crankshaft/bearings forces. It can be seen for the two operating points that gas/cylinder head forces are non-negligible only in low frequency, up to the 500 Hz band for operating point (3500 rev/min/164 Nm) and upto the 750 Hz band for operating point (1400 rev/min/23 Nm). Secondly, we note that the partial response to the crankshaft/bearing forces is the most important one above 500 Hz for both operating points. Partial response to piston/cylinder forces is significant, for both operating

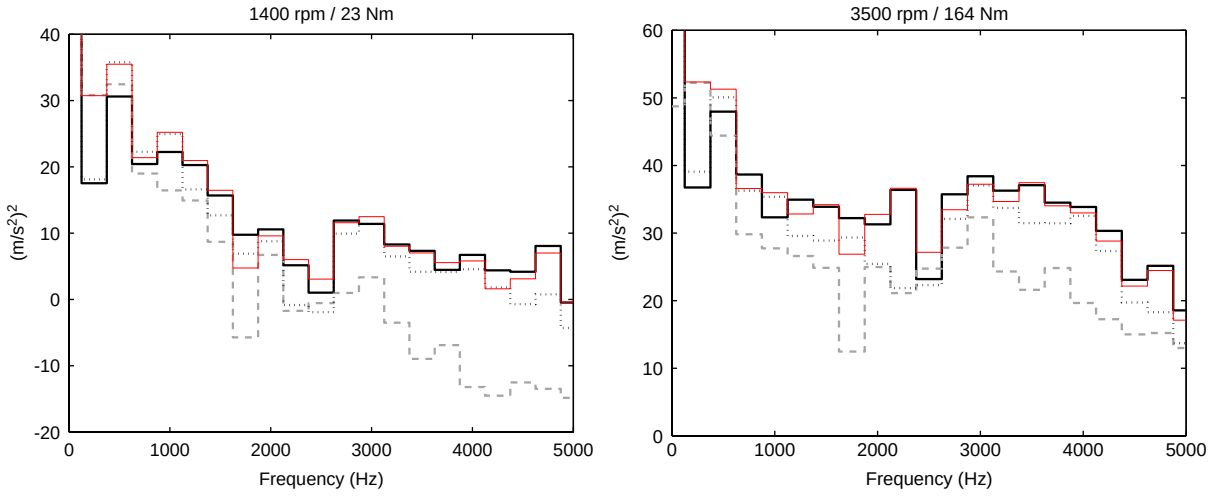

Fig. 14. Contributions of gas/cylinder head - -, pistons/cylinders ···, and cranshaft/bearings excitations — to the acceleration at the belt side engine mount for operating points (1400 rev/min/23 Nm) (left) and (3500/164 Nm) (right). ___: total response.

points, between 500 Hz and 1 kHz and between 2750 and 4250 Hz. Meanwhile, these results are conditioned by the suspected poor quality of identified piston/cylinder forces.

4. Conclusions

The results that are presented in the final section demonstrate the use of inverse analysis in recovering forces exciting structures from acceleration measurements. The inverse methodology exposed in the first part has shown its efficiency in a complex application: the diesel engine. It has been shown that the optimization and regularization steps are essentials to ensure an optimal inversion of the transfer system. It has been shown that the direct measurement of some of the excitations (cylinder pressures) can easily be introduced in the method, improving the identification of other forces. Indirect measurement results allow one to rank the contributions of reconstructed excitations to the structure response. Moreover, it is a precious tool to assess the validity of excitation models, or to identify mechanical systems transmitting source forces (e.g. combustion) to induced forces (e.g. bearings loads). Some simple principles have to be carefully observed when implementing such methods. Firstly, a special effort has to be given to the modeling step, because slight differences between the transfer model and the real system can strongly influence the identified forces. If the transfer matrix comes from a finite element model, it is sure that a strong updating step is needed. Secondly, response sensors have to be placed as close as possible to excitations to optimize the conditioning of the transfer system. Thus, sensors have been placed on bearing caps of the diesel engine, leading to successful identification of bearing loads. Forces identified on the cylinders have not been as satisfying, because of the location of allocated accelerometers (on the external face of the engine) that was not optimized. An optimal

location would have been the placing of four accelerometers on the external faces of the four cylinders through the cooling water, involving a more complex instrumentation.

Acknowledgements

This work has been carried out in the frame of a Ph.D. Thesis [9] has been financed by Renault.

References

[1] S.M. Price, R.J. Bernhard, Virtual coherence: a digital signal processing technique for incoherent source identification, in: *Proceedings of IMAC 4*, Schenectady, NY, USA, 1986.
[2] Q. Leclere, C. Pezerat, B. Laulagnet, L. Polac, Different least squares approaches to identify dynamic forces acting on an engine cylinder block, *Acta Acustica united with Acustica* 90 (2) (2004) 285–292.
[3] M.H.A. Janssens, J.W. Verheij, A pseudo-forces methodology to be used in characterization of structure-borne sound sources, *Applied Acoustics* 61 (3) (2000) 285–308.
[4] Q. Leclere, C. Pezerat, B. Laulagnet, L. Polac, Reconstitution of stationary forces exciting an engine cylinder block, in: *Proceedings of Inter-Noise 2002*, Dearborn, MI, USA, August 2002.
[5] P.C. Hansen, The 1-curve and its use in the numerical treatment of inverse problems [on line], ⟨http://citeseer.nj.nec.com/196586.html⟩.
[6] M.H.A. Janssens, J.W. Verheij, T. Loyau, Experimental example of the pseudo-forces method used in characterization of a structure-borne sound source, *Applied Acoustics* 63 (2002) 9–34.
[7] A.N. Thite, D.J. Thompson, The quantification of structure-borne transmission paths by inverse methods, Part 1: improved singular value rejection methods, *Journal of Sound and Vibration* 264 (2003) 411–431.
[8] H.R. Busby, D.M. Trujillo, Optimal regularization of an inverse dynamics problem, *Computers and Structures* 63 (2) (1997) 243–248.
[9] Q. Leclere, Etude et Developpement de la Mesure Indirecte d'Efforts—Application à l'Identification des Sources Internes d'un Moteur Diesel, Ph.D. Thesis, INSA Lyon, 2003.
[10] B. Swoboda, *Mécanique des Moteurs Alternatifs*, Technip, Paris, 1984.
[11] J. Van Herbruggen, P.J.G. Van der Linden, F. Deblauwe, H.J. Knittel, J. Schnur, Engine internal dynamic force identification and the combination with engine structural and vibro-acoustic transfer information, in: *Proceedings of ICSV 8*, Hong Kong, China, July 2001.